Diversity and Hierarchy in Supramolecular Assemblies of Triphenylalanine: From Laminated Helical Ribbons to Toroids

Enric Mayans,[1,2] Jordi Casanovas,[3] Ana M. Gil,[4] Ana I. Jiménez,[4] Carlos Cativiela,[4,*] Jordi Puiggalí,[1,2,*] and Carlos Alemán[1,2,*]

[1] *Departament d'Enginyeria Química, EEBE, Universitat Politècnica de Catalunya, Edifici I.2, C/ Eduard Maristany, 10-14, 08019, Barcelona, Spain*

[2] *Research Center for Multiscale Science and Engineering, Universitat Politècnica de Catalunya, C/ Eduard Maristany, 10-14, 08019, Barcelona, Spain*

[3] *Departament de Química, Escola Politècnica Superior, Universitat de Lleida, c/ Jaume II nº 69, Lleida E-25001, Spain*

[4] *Department of Organic Chemistry and Instituto de Síntesis Quimica y Catalisis Homogenea (ISQCH), Universidad de Zaragoza–CSIC, 50009 Zaragoza, Spain*

[*] jordi.puiggali@upc.edu, cativiela@unizar.es and carlos.aleman@upc.edu

ABSTRACT

Microstructures from small phenylalanine-based peptides have attracted great attention lately since these compounds are considered as a new class of tunable materials. In spite of the extensive studies on uncapped diphenylalanine and tetraphenylalanine peptides, studies on the self-assembly of uncapped triphenylananine (FFF) are very scarce and non-systematic. In this work we demonstrate that FFF assemblies can organize in a wide number of well-defined supramolecular structures, which include laminated helical-ribbons, leave-like dendrimers, doughnut-, needle- and flower-shapes. These organizations are produced by the attractive or repulsive interactions between already formed assemblies and, therefore, can be controlled through the choice of the solvents used as incubation medium. Thus, the formation of desired supramolecular structures is regulated through the protonation / deprotonation of the terminal groups, the polarity of the incubation medium, which affects both peptide···solvent interactions and the cavity solvation energy (*i.e.* solvent···solvent interactions), and the steric interactions between the own assemblies that act as building blocks. Finally, the β-sheet disposition in the latter structural motives has been examined using both theoretical calculations and FTIR spectroscopy. Results indicate that FFF molecules can adopt both parallel and antiparallel β-sheets. However, the former one is the most energetically favored due to the formation of π-π stacking interactions between the aromatic rings of hydrogen bonded strands.

INTRODUCTION

Reches and Gazit reported in 2003 the self-assembly of diphenylalanine (FF) into well-ordered nanotubes.[1] Since then, small phenylalanine-based aromatic peptides have been considered as a new class of materials owing to their structural simplicity and tunability, functional versatility, cost effectiveness, and widespread applications.[2-4] However, despite the enormous effort devoted to study the self-assembly of small peptides containing the FF-sequence,[5-10] research on phenylalanine-homopeptides is still incomplete. Thus, recent studies have evidenced that phenylalanine-homopeptides can exhibit structural and morphological variability, which has been found to depend on the number of phenylalanine residues and the capping groups used for the complete elimination of the normally free basic (N-terminus) and acidic (C-terminus) ends.

The main aims of this investigation are two. The first is to precisely control the structure of uncapped phenylalanine-homopeptides, which have been shown a preference towards the tube like-morphology, controlling the molecular self-assembly and/or the hierarchical supramolecular organization of the pre-formed tubular assemblies through the polarity of the incubation medium. The second is to consider an homopeptide with an odd number of phenylalanine residues to complement previous investigations on FF[1,2] and FFFF.[11] Thus, comparative studies suggested significant structural differences depending on the even or odd number of phenylalanine residues for homopeptides with identical blocking groups.[12] In order to combine such two objectives, in this work we examine the assembly of uncapped FFF (Scheme 1), which despite its simplicity has been scarcely studied. For this purpose, after summarize the antecedents for FF, FFF and FFFF, and the Methods in the next two sections, we report an exhaustive morphological analyses for FFF. Results demonstrate the very remarkable influence of the incubation conditions in the hierarchical assembly of the

homotripeptide, regulating the formation of stable structural building blocks that subsequently organize in supramolecular polymorphs. In addition, both theoretical calculations on small model complexes and FTIR spectroscopy studies in different environments provide deeper understanding on the arrangement of the FFF molecules in the β-sheets formed in the assembly process.

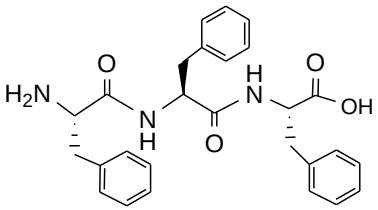

Scheme 1

ANTECEDENTS: FF, FFF AND FFFF ASSEMBLIES

Tubular nanostructures free of defects have been typically reported for FF, which form spontaneously and efficiently upon the peptide dilution from organic solvents into aqueous solution.[1,2,11,13-16] FF nanotubes present remarkable stiffness, mainly attributed to intermolecular hydrogen bonding and aromatic interactions[17,18] and the water molecules inside the peptide nanochannels.[19] Moreover, these nanostructures are stable not only in dry but also in solution conditions,[20,21] and displayed intrinsic luminescence[22] and piezoelectric properties.[23]

In some conditions nanotubes are not formed discretely but grouped into supramolecular organizations. For example, diluted FF solutions in hexafluoroisopropanol (HFIP):water and dimethylformamide (DMF):water mixtures at 4 ºC give place to nanotubes growing from dendritic hyperbranched structures, which transform into spherulitic nucleus-like shapes when the temperature increases to 25 ºC.[11] The definition of FF tubes improves in HFIP:ethanol (EtOH) solutions at 4 ºC, while dimethylsulfoxide (DMSO):water promotes the crystallization of FF.[11,24] Ihee and

co-workers demonstrated that, in aqueous phase at high ionic strength, FF adopts nanowire morphologies, which can be readily disintegrated and used to form nanotubes by adjusting the aqueous conditions of preparation.[25] Furthermore, unilocular and multilocular FF hollow spheres were recently achieved by Zhu and co-workers[26] using surfactant-free emulsion droplets as the template and glutaraldehyde as the crosslinking agent.

On the other hand, studies on the self-assembly of FFF[27-29] and FFFF[11] are very scarce. Tamamis *et al.*[27] examined the aggregation of FFF in HFIP:water at a concentration of 2 mg/mL. Results indicated that this tripeptide organizes into plate-like nanostructures rich in β-sheet content, even though no other experimental condition was investigated.[27] In a very recent study, toroid nanostructures were obtained by the co-assembly of FF and FFF at various mass ratios in 4% HFIP aqueous solutions with a total peptide concentration of 4 mg/mL.[28] Also, computer simulation studies based on molecular dynamics (MD) with classical force fields predicted that FFF can self-assemble into solid densely packed nanospheres and nanorods.[29]

The organization of FFFF in tubular microstructures was exhaustively examined in a recent study by considering a wide number of incubation conditions.[11] FFFF assembles into relatively short and well-defined tubes (diameter, ϕ= 0.58±0.12 μm, and length, L, ≤ 100 μm) at 4 ºC in HFIP:EtOH solutions with peptide concentrations ranging from 1 to 2 mg/mL. Both the length and abundance of such tubes increase noticeably when the EtOH co-solvent was replaced by water (ϕ ranging from ~50 to ~700 nm and L > 200 μm). DMF:water promoted the formation of tubular structures at 4 ºC when the peptide concentration ranges from 0.1 to 0.5 mg/mL, while meta-stable tube-like assemblies (*i.e.* aggregates at the early stages of the nanotube-formation process) were obtained at lower concentrations. Independently of both the solvent and the peptide concentration,

FFFF tubes showed birefringence using cross polarized light illumination, indicating that peptide molecules retain the same orientation along the whole assembly.[11]

Additionally, several investigations on FFFF-polymer conjugates have been reported in the last years.[30-33] FFFF-polyethylene glycol (PEG) conjugates associate into irregular aggregates at low concentration and into well-developed β-sheets at high concentration.[30] Furthermore, the drying of FFFF-PEG solutions resulted in the crystallization of PEG without disrupt the local β-sheet structure defined by the peptide block, the independent organization of the two FFFF-PEG counterparts being studied at the microscopic level using atomistic MD simulations.[31] On the other hand, the assembly of FFFF-poly(ethylene oxide) (PEO) conjugates, which were prepared by click chemistry, was found to depend on the polymer length.[32,33] Nanotubes formed by anti-parallel β-sheets were observed for short PEO blocks while hybrids with longer polymer blocks gave rise to fibres and worm-like micelles.

METHODS

Peptide synthesis. Melting points were determined on a Gallenkamp apparatus and are uncorrected. IR spectra were registered on a Nicolet Avatar 360 FTIR spectrophotometer; ν_{max} is given for the main absorption bands. ^{1}H and ^{13}C NMR spectra were recorded on a Bruker AV–400 instrument at room temperature, using the residual solvent signal as the internal standard; chemical shifts (δ) are expressed in ppm and coupling constants (*J*) in Hertz. Optical rotations were measured with a JASCO P-1020 polarimeter. High-resolution mass spectra were obtained on a Bruker Microtof-Q spectrometer.

The synthetic strategy used to prepare FFF is shown in Scheme 1.

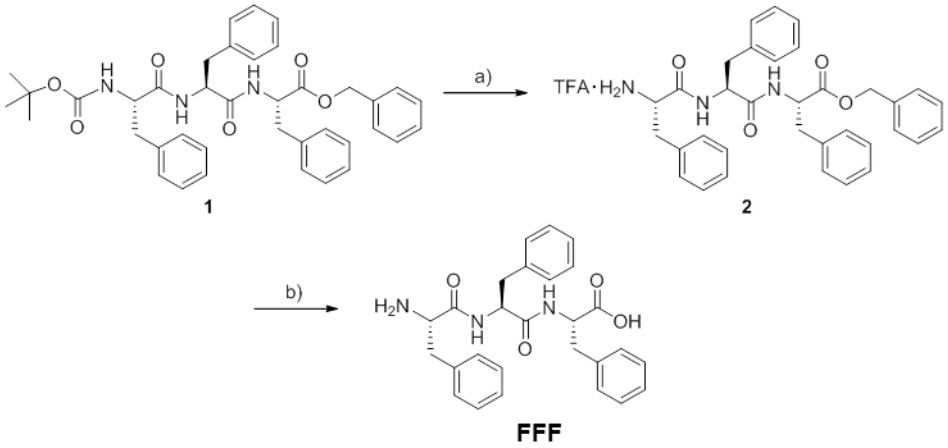

Scheme 1. Reagents and conditions: (a) TFA, CH_2Cl_2, rt 2 h; (b) H_2/Pd, MeOH, rt, 2h.

TFA·H-L-Phe-L-Phe-L-Phe-OBzl (2)

A solution of Boc-L-Phe-L-Phe-L-Phe-OBzl (**1**)[11] (2.0 g, 3.1 mmol) in dichloromethane (30 mL) was treated with trifluoroacetic acid (5 mL) and the reaction mixture was stirred at room temperature for 2 h. After evaporation of the solvent, the residue was suspended in a diethyl ether/*n*-hexane mixture and filtered at reduced pressure to provide the corresponding trifluoroacetate salt **2** as a white solid in quantitative yield.

2: Mp: 190-192 ºC. $[\alpha]_D^{21}$: -5.4 (c = 0.50, methanol). IR (neat) *ν*: 3139, 1728, 1698, 1645 cm^{-1}. ^1H NMR (MeOH-d_4, 400 MHz): δ 2.84 (dd, 1H, *J* = 13.8 Hz, *J* = 8.8 Hz), 2.90 (dd, 1H, *J* = 14.1 Hz, *J* = 8.6 Hz), 3.01 (dd, 1H, *J* = 13.9 Hz, *J* = 8.1 Hz), 3.08 (dd, 1H, *J* = 14.1 Hz, *J* = 5.7 Hz), 3.12–3.19 (m, 2H), 4.00 (dd, 1H, *J* = 8.9 Hz, *J* = 4.9 Hz), 4.68–4.73 (m, 2H), 5.07–5.14 (m, 2H), 7.16–7.36 (m, 20H). ^{13}C NMR (MeOH-d_4, 100 MHz): δ 38.45, 38.58, 39.02, 55.34, 55.50, 55.94, 68.06, 113.75, 116.70, 119.61, 122.51, 127.83, 127.90, 128.81, 129.38, 129.49, 129.55, 130.10, 130.25, 130.34, 130.50, 135.39, 136.93, 137.86, 138.01, 162.33, 162.68, 163.03, 163.37, 169.39, 172.33, 172.87. HRMS (ESI) $C_{34}H_{35}N_3NaO_4$ $[M+Na]^+$: calcd. 572.2520, found 572.2526.

H-L-Phe-L-Phe-L-Phe-OH (FFF)

A solution of compound **2** (1.10 g, 1.7 mmol) in methanol (30 ml) was hydrogenated at atmospheric pressure for 2 h using 10 % Pd-C (100 mg) as a catalyst. The mixture was filtered through Celite and the solvent was removed at reduced pressure. A suspension in water (10 mL) of the trifluoroacetate salt obtained was treated with *N*-methylmorpholine (NMM) (0.22 mL, 2.0 mmol). The resulting solid was filtered and washed with diethyl ether to provide FFF as a white solid in nearly quantitative yield

FFF: Mp: 218-219 ºC. $[\alpha]_D^{20}$: 26.3 (c = 0.37, acetic acid). IR (neat) ν: 3360, 1654 cm^{-1}. HRMS (ESI) $C_{27}H_{29}N_3NaO_4$ $[M+H]^+$: calcd. 482.2050, found 482.2026. (Due to poor solubility it was impossible to record the NMR spectra in typical NMR solvents, therefore we recorded the NMR spectra of the TFA salt).

TFA·FFF: ^{1}H NMR (DMSO, 400 MHz): δ 2.77–3.02 (m, 4H), 3.04–3.13 (m, 2H), 3.94–4.04 (m, 1H), 4.51 (dt, 1H, *J* = 8.4 Hz, *J* = 5.1 Hz), 4.63 (dt, 1H, *J* = 8.7 Hz, *J* = 4.5 Hz), 7.17–7.30 (m, 15H), 8.04 (bs, 3H), 8.57 (d, 1H, *J* = 7.8 Hz), 8.79 (d, 1H, *J* = 8.2 Hz). ^{13}C NMR (DMSO, 100 MHz): δ 36.71, 37.00, 37.69, 53.08, 53.54, 54.03, 112.23, 115.17, 118.12, 121.07, 126.45, 127.11, 128.15, 128.23, 128.48, 129.14, 129.28, 129.61, 134.70, 137.39, 137.47, 157.73, 158.06, 158.39, 158.72, 167.89, 170.65, 172.66.

Preparation of initial solutions. Organic solvents for preparing peptide solutions were purchased from Sigma-Aldrich. FFF stock solutions were freshly prepared dissolving 5 mg/mL in hexafluoroisopropanol (HFIP). Peptide stock solutions were diluted in double distilled water, methanol (MeOH) or isopropanol (^{i}PrOH) to a final concentration ranging from 4 mg/mL and 0.05 mg/mL was added to assist in the

surface-mediated assembly process. Finally, 10-20 μL aliquots of peptide solution were drop-casted on microscope glass coverslips and kept at 4 ºC inside a cold chamber until dryness.

Optical microscopy. Morphological observations were performed using a Zeiss Axioskop 40 microscope. Micrographs were taken with a Zeiss AxiosCam MRC5 digital camera.

Scanning electron microscopy (SEM). SEM studies were performed in a Focussed Ion Beam Zeiss Neon 40 scanning electron microscope operating at 5 kV and equipped with an EDX spectroscopy system. Samples were mounted on a double-side adhesive carbon disc and sputter-coated with a thin layer of carbon to prevent sample charging problems.

Atomic Force Microscopy (AFM). Topographic AFM images were obtained using either a Dimension 3100 Nanoman AFM or a Multimode, both from Veeco (NanoScope IV controller) under ambient conditions in tapping mode. AFM measurements were performed on various parts of the morphologies, which produced reproducible images similar to those displayed in this work. Scan window sizes ranged from 3×3 μm^2 to 20×20 μm^2.

Theoretical calculations. Density Functional Theory (DFT) calculations were performed using the Gaussian 09 computer package.[34] The geometries of the different investigated systems were fully optimized using the M06L[35,36] functional, which was

developed by Zhao and Truhlar to account for dispersion, combined with the 6-31+G(d,p) basis set. No symmetry constraints were used in the geometry optimizations.

Complexes formed by three and four FFF molecules were considered. The interaction energy, ΔE_{int}, for each complex was computed as:

$$\Delta E_{int} = E(complex) - n \times E(peptide) \quad (1)$$

where E(peptide) is the energy of the single peptide molecule after complete geometry optimization and *n* is the number of peptide molecules in the complex.

The cooperative energy, ΔE_{coop}, which provides an evaluation of the many-body (non-additive) effects, was estimated as the difference between ΔE_{int} and the expected interaction energies, $\Delta E_{int}(E)$. The latter value was calculated considering the sum of the interaction energies of all dimers contained in the complex. As example, for a complex containing three FFF molecules $\Delta E_{int}(E)$ and ΔE_{coop} can be defined as follows:

$$\Delta E_{coop} = \Delta E_{int} - \Delta E_{int}(E) \quad (2)$$

where

$$\Delta E_{int}(E) = \Delta E_{int}\,(1\text{-}2) + \Delta E_{int}\,(2\text{-}3) + \Delta E_{int}\,(1\text{-}3) \quad (3)$$

$$\Delta E_{int}\,(1\text{-}2) = E(dimer\ 1\text{-}2) - 2\times E(peptide) \quad (4)$$

$$\Delta E_{int}\,(2\text{-}3) = E(dimer\ 2\text{-}3) - 2\times E(peptide) \quad (5)$$

$$\Delta E_{int}\,(1\text{-}3) = E(dimer\ 1\text{-}3) - 2\times E(peptide) \quad (6)$$

In all cases interaction energies were corrected with the basis set superposition error (BSSE) by mean of the standard counterpoise method.

FTIR spectroscopy. Infrared transmittance spectra were recorded with a Jasco FTIR 4100 Fourier Transform spectrometer in a 4000-650 cm^{-1} interval. An MKII Golden

Gate attenuated total reflection (ATR) accesory from Specac was used. The measurements were taken using 4 cm^{-1} resolution and 1000 scans averaging.

RESULTS AND DISCUSSION

The polymorphism of self-assemblies is known to depend on both the peptide concentration and the polarity of the medium.[37-39] The influence of both variables can be simultaneously examined adding a co-solvent to a peptide stock solution, even though interpretation of the role played by each factor in the assembly process becomes a difficult task. In order to facilitate the understanding of the results, in this work we have used three different co-solvents with diverse dielectric constants (*i.e.* ε= 78.3, 32.6 and 17.9 for water, MeOH and ^{i}PrOH, respectively) for addition to the HFIP (ε= 16.7) stock solution. This solvent:co-solvent strategy has enabled us to contrast the effects of solvents mixtures with similar polarities, which are made with different co-solvents and, therefore, necessarily involve very different concentrations.

FFF dissolved in HFIP:water with concentrations ranging from 2 to 4 mg/mL (*i.e.* from 4:6 to 4:1 HFIP:water ratios) self-assembles into plate-like microstructures at 4 ºC (Figures 1a and S1). The characteristic planar shape of these structures is very similar to that found by Tamamis *et al.*[27] using analogous experimental conditions. The length of the plates is around 7 μm while the width and the height, which were determined by AFM (Figure S2), is around 700 and 400 nm, respectively. Birefringent microplates are retained when the peptide concentration ranges from 0.5 to 2 mg/mL (*i.e.* from 1:9 to 4:6 HFIP:water ratios), even though the surface becomes less smooth with decreasing FFF concentration. Moreover, microplates with well-defined twists along the plate axis are detected, its frequency increasing with decreasing peptide concentration. The shape of such twists, which resemble those found in β-amyloid fibres,[40-42] is illustrated in

Figure 1b for 0.5 mg/mL HFIP:water (1:9) solution. The apparition of twisting in the microplates suggests that the ionization of the FFF molecules, which is caused by the addition of water to the stock HFIP solution, introduces distortions in the associated β-sheets or even in the own β-strands. Apparently, such distortion events are non-systematic for 0.5-2 mg/mL peptide concentrations (*i.e.* 1:9-4:6 HFIP:water ratios) since no defined periodicity has been observed for the twists.

In contrast, discrete microfibrils with well-defined helical ribbons are obtained when the peptide concentration decreases to 0.05 mg/mL (*i.e.* 1:99 HFIP:water ratio). The average length of these regular structures, which display only one twist axis along the long helical axis (n_l in Figure 1c), is ~230 μm. The half pitch length along the n_l axis, which requires a twist of 180º, is ~50 μm, while the length of the helical fibril along the short helix (n_s in Figure 1c) is ~5.5 μm. High resolution SEM micrographs show that fibrils contain a very large number of laminates, resembling amyloid fibril lamination.[40,43] Fibrils formed by long β-amyloids are usually involve around 24 laminates,[43] while in this case they are much more extensive. However, up to 130 laminates, which were 130 nm wide each, were reported for FF-containing fibrils prepared using the CH_3CO-KLVFFAE-NH_2 peptide.[40] In the present work, laminates obtained for FFF are ~320 nm wide. Overall, results displayed in Figure 1 reflect that the transformation from flat plates to laminated helical fibrils is caused by the progressive addition of water to the stock FFF solution, which causes both the enhancement of the medium polarity and the ionization of the uncapped peptide ends.

Dilution of the stock HFIP peptide solutions with MeOH led to the formation of supramolecular structures that are completely different from those incubated in HFIP:water mixtures. More specifically, OM and SEM micrographs with increasing magnification of structures derived from 4 mg/mL HFIP:MeOH (4:1) peptide solutions

(Figure 2a) show groups of well-defined needle-like microstructures growing from a common nucleus, each needle being a supramolecular assembly of ultra-thin nanoplates. AFM images (Figure 2b) corroborates such supramolecular organization. Comparison of these structures with those displayed in Figures 1a and S1 reflects that the reduction of the solution polarity causes not only a drastic shortening of the plates' length and width (the depth is very thin in both cases) but also a subsequent supramolecular ordering.

The supramolecular organization of nanoplates is lost when the polarity of the medium increases through the addition of more MeOH. Thus, the structures obtained using HFIP:MeOH solutions with a peptide concentration comprised between 2 and 0.5 mg/mL (*i.e.* between 4:6 and 1:9 HFIP:MeOH ratios) resemble the aggregates of microplates derived from HFIP:water solutions. This is reflected by the OM and SEM micrographs of representative structures found for 2.0 and 0.5 mg/mL HFIP:MeOH (4:6 and 1:9 HFIP:MeOH, respectively) peptide solutions (Figure S3). The very planar surface of the microplates achieved using such relatively diluted peptide solutions contrasts with the rough surface of the microstructures constituted by ordered assemblies of nanoplates, as is evidenced by comparing the AFM images displayed in Figures 2b and S3b. The influence of the polarity of the incubation medium in the plate-containing structures of FFF is schematically depicted in Figure 3a. Although measurement of the dielectric constant of the mixtures used to promote the self-assembly and supramolecular organization of FFF is out of the scope of this work, it is worth noting that the polarity of the medium strongly influences such processes. Early studies suggested that the dielectric constant of mixed solvents can be predicted as the weighted average of the mixture components by assuming that solvents behave ideally (*i.e.* a simple additive function of the concentration of the solvents).[44,45] However, more

recent investigations have proved a high degree of intermolecular interactions, evidencing a non-ideal behavior.[46] Accordingly, sophisticated models and accurate oscillometry measurements would be required to estimate quantitatively the polarity each medium. However, considering that the differences in the dielectric constants of the solvents used in this work are significant, quantitative values are not necessary to understand the structural differences discussed above.

According to these observations, the formation of FFF plates at different length-scales depends on the kinetic or thermodynamic control of the assembly process. In polar environments (*i.e.* HFIP:water and HFIP:MeOH with a high content of MeOH), FFF molecules diffuse to participate in the growing of already nucleated microplates. The assembly process follows a thermodynamic mechanism, prioritizing the stability of the already formed structures with respect to the continuous formation of crystallization nuclei. In opposition, a multinuclear kinetic mechanism is preferred in non-polar environments (*i.e.* HFIP:MeOH with a low content of MeOH), the growing of large and stable planar crystals being not preferred with respect to the formation of additional crystallization nuclei.

Reduction of the peptide concentration to 0.1 and 0.05 mg/mL (*i.e.* 1:49 and 1:99 HFIP:MeOH ratios, respectively) enabled the formation of microstructures with completely different shapes. The most abundant one corresponds to the doughnut-shape, or toroidal, morphology (Figure 4a) with diameter typically comprised between 2 and 4 µm. Due to the low peptide concentration, the abundance of these structures, which were randomly distributed onto the surface, was relatively poor. The fact that doughnut-like hollow microstructures displayed a significant variability in the wall-thickness suggests that this morphology is probably originated by a solvent-driven mechanism (discussed below). It is worth noting that doughnut-like structures were also obtained by

co-assembling FF and FFF in a HFIP:water.[28] In this case, the diameter of the structures was regulated through the FF:FFF mass ratio: the formation of micro-doughnuts (diameters similar to those displayed in Figure 4a) was dominated by FF···FFF interactions, while the apparition of nano-doughnuts (diameter < 200 nm) was favored by the competition between FF···water and FFF···water interactions.

On the other hand, with relative frequency micro-bottles grew from bottom to the top through the stacking of individual doughnut-shape structures (Figure 4b), confirming that the latter are formed in the solution phase. AFM images indicate that such microstructures are randomly distributed in the surface without following any regular apparition and growing pattern. The formation of micro-bottles has been attributed to the stability of hydrophobic peptide···peptide interactions between molecules belonging to different microstructures, which compete against both peptide···surface and solvent···surface interactions. Thus, once the micro-doughnut is formed in solution, it prefers to deposit onto an already formed peptide microstructure, giving place to the formation of the micro-bottle, than onto the hydrophilic glass substrate. The fact that the concentration of peptide is very small seems to be what prevents a greater abundance of micro-bottles.

OM and SEM micrographs (Figures 5 and S4) of assemblies formed at 4º C from concentrated (*i.e.* 4 mg/mL) 4:1 HFIP:^{i}PrOH peptide solutions reflect the presence of coexisting dendritic and doughnut-like structures. The most representative characteristics of the dendritic structures are their large dimensions, birefringence, and leaves-like morphology. However, such huge structures are inhibited by diluting the peptide solution through the addition of more ^{i}PrOH, indicating that their formation is mainly driven by a peptide concentration gradient in a mixture of solvents with low dielectric constant (*i.e.* 17.9 and 16.7 for ^{i}PrOH and HFIP, respectively). In contrast,

doughnut-like structures, which are very stable (*i.e.* the AFM image included in Figure 5b was taken from a sample stored for more than 6 months), are observed even when the peptide concentration decreases to 0.05 mg/mL (1:99 HFIP:^{i}PrOH). The diameter of the doughnut-shape microstructures is around 14-15 μm while the wall-thickness is 4-5 μm. These dimensions are clearly reflected in Figure 5b, which displays the AFM cross-sectional profile of a representative microstructure. Accordingly, doughnut-like microstructures obtained in HFIP:^{i}PrOH solutions are several times bigger, independently of the peptide concentration, than those formed in very diluted HFIP:MeOH solutions.

The observation of some compact and densely packed microstructures suggests that such hollow doughnut-like structures are formed through a solvent-driven mechanism, like that schematically depicted in Figure 5c. The formation of compact structures at the initial stages has been attributed to the fact that peptide···peptide interactions, which are probably dominated by side chain···side chain aromatic stacking, are slightly stronger than peptide···solvent. However, the contribution of the cavity solvation energy, which depends on the strength of solvent···solvent interactions, to the total potential energy of the system and the dynamical competition between peptide···peptide and peptide···solvent interactions result in the formation of hollow microstructrures. Thus, ^{i}PrOH and HFIP can promote the formation of two types of peptide···solvent interactions through their hydroxyl and alkyl groups: *i)* (solvent)O–H···O=C(peptide) hydrogen bonds, which are slightly weaker (peptide)N–H···O=C(peptide) interactions;[47] and *ii)* van der Waals interactions, which are weaker than peptide···peptide stacking interactions.[48]

The same mechanism is probably responsible of the formation of doughnut-shape microstructures in HFIP:MeOH. Differences in the diameters of microstructures

obtained in HFIP:^{i}PrOH and HFIP:MeOH, which are apparently independent of the peptide concentration, should be attributed to the influence of the polarity of the medium (*i.e.* the dielectric constant of ^{i}PrOH and MeOH is 17.9 and 32.6, respectively). The growing of the initial densely packed microstructures (*i.e.* before the formation of the hollow), which define the diameter of the subsequently formed hollow microstructures, is severely restricted by repulsive peptide···solvent interactions at the border. Accordingly, the diameter grows when polarity of the medium and, therefore, the repulsive character of peptide···solvent interactions, decrease.

Reduction of the peptide concentration dissolved in 4:6 HFIP:^{i}PrOH to 2 mg/mL results in a drastic change (Figure 6a). The peptide self-assembles into a variety of morphologies that share a characteristic trend: they are all based on the aggrupation of microplates of similar dimensions (*i.e.* ~30 and ~3 μm of length and width, respectively) as a basic motif. Thus, low and high resolution SEM micrographs reveals the coexistence of discrete microplates, groups involving a different number of assembled microplates and large clusters of microplates organized into well-defined supramolecular structures with a flower-like morphology, that in turn can be observed alone or assembled in small groups. Indeed, all these structures correspond to different degrees in the hierarchical assembly of microplates, which act as building blocks.

The mechanism associated to the hierarchical formation of flower-shaped clusters is illustrated in Figure 3b. We hypothesize that the assembly of FFF microplates is mediated by a balance between attractive interactions and steric hindrance. The agglomeration of well-defined microplates indicates that there are attractive interactions among them, possibly mediated not only by the aromatic side groups of Phe residues but also by other attractive forces involving the termini groups of FFF molecules located at different basic motifs. It should be noted that the moderate concentration of

peptide molecules in the HFIP:^{i}PrOH favors the growth of microplates with respect to nanoplates since the latter requires a very fast and abundant formation of nuclei at the first stage of the assembly process. The assembly of microplates originates a twisting effect, which is probably due to the accommodation of the building blocks favoring the attractive interactions with respect to the repulsive ones. Moreover, the irregular growing of clusters from such twisted assemblies originates the apparition of empty regions at the edges because of the interlocking of the elongated microplates. The sides of clusters are sterically hindered by the assembled microplates, which prevent access of additional assemblies at the same plane. Thus, the aggrupation of microplate assemblies results in the hierarchical growing of 3D clusters with flower-like morphology. The growing of each 3D cluster, which resembles a chrysanthemum, is restricted by both the size the building blocks (*i.e.* length and width of microplates) and the number assemblies that can be accommodated inside this regular network structure. Finally, attractive interactions between microplates located at different 3D clusters cause their grouping in small sets of two or three flower-like structures.

The reduction of the peptide concentration to 0.5 mg/mL (1:9 HFIP:^{i}PrOH) favors the formation of smaller crystalline plates (*i.e.* ~3 and ~1 μm of length and width, respectively; Figure S5), affecting in turn the flower-like morphology that becomes less precise (Figure 6b). These microstructures are still present when the peptide concentration decreases to 0.1 and 0.05 mg/mL (*i.e.* 1:49 and 1:99 HFIP:^{i}PrOH ratios, respectively), even though the poorly defined doughnut-shape morphology is the most abundant (Figures S6 and S7). Thus, the hollow is quite irregular, the wall thickness is not uniform (*e.g.* it ranges from 500 nm to 1.3 μm for 0.1 mg/mL peptide solutions in 1:49 HFIP:^{i}PrOH), and the diameter is significantly lower than those observed for concentrated peptide solutions (Figures 5b-c).

Guo *et al.*[29] recently examined the self-assembly of FFF in water using MD simulations and coarse-grained models, in which each phenylalanine residue was represented by four beads (*i.e.* one bead for the main chain and three beads for the side chain ring structure) and groups of four water molecules were described with a single bead. Therefore, predictions should be considered qualitatively because of the simplified definition of the chemical characteristics of the modeled system (*e.g.* omission of the protonation of the terminal groups and poor representation of the interactions at the first solvation shell). Results indicated that FFF peptides spontaneously assemble into nanorods and nanospheres in aqueous environments.[29] The formation of such nanostructures was mainly attributed to stability of the resulting β-sheets and to the peptide···solvent interactions. It is worth noting that, although both length- and time-scales are not comparable, the simulated assemblies resemble some of the structures experimentally found in HFIP:MeOH and HFIP:^{i}PrOH. Thus, the characteristics of the predicted nanorods are pretty similar to those of nano- and microplates, while modeled nanospheres are comparable to the compact structures associated to initial stages of the hollow microstructures formation. Unfortunately, modeling of supramolecular structures like those reported in this work is currently impossible due to the huge amount of computational resources required for such purpose. However, coarse-grained models are suitable to provide preliminary information about the initial stages of self-assembly of small peptides, which can be useful for *de novo* design of new supramolecular structures.

Comparison of the structures obtained in this work for FFF with those reported for FF and FFFF using the same experimental conditions reflect the importance of the peptide length in the self-assembly process.[11] More specifically, two main factors are related with the self-assembly ability of such three peptides. Firstly, the role played by

electrostatic, hydrogen bonding and π-π stacking interactions, which are associated to the charged N- and C-terminus, the amide groups and the phenyl side chains, respectively. Thus, the relative importance of the electrostatic interactions with respect to the hydrogen bonding and π-π stacking ones decreases with increasing peptide length. Secondly, the conformational flexibility of the peptide increases with the peptide length. The balance between such two factors affects to the definition (*e.g.* irregularities in tubular structures increases as follows:[11] FF < FFF < FFFF), or even the disappearance (*e.g.* hyperbranched structures have been observed for FF[11] and FFF – this work – but not for FFFF[11]), of some polymorphic forms.

By analogy with FF[1,2,11,13-16] and FFFF,[11] FFF structures are expected to be formed by β-sheets (this assumption is proved below by FTIR spectroscopy). Moreover, the different basic motifs observed in this work (*e.g.* fibers and plates) probably differ in the packing mode of such β-sheets. Recent studies on different small peptides demonstrated that the morphology of basic motifs is frequently due to changes in the packing mode of β-sheets rather than to drastic changes in the molecular conformation.[11,49] On the other hand, supramolecular assemblies derived from the same basic motif are expected to preserve the packing of the β-sheets. According to this features, microscopy observations discussed in this work have been completed by examining the parallel or antiparallel disposition of β-sheets formed by FFF strands using both theoretical calculations and FTIR spectroscopy.

Firstly, DFT calculations were performed considering sheets involving model complexes with 3 or 4 β-strands in the gas-phase. For this purpose, calculations were carried out considering different starting arrangements for each system (*i.e.* more than 9 per disposition), which were constructed by introducing small variations in the dihedral angles to improve the geometry of intermolecular hydrogen bonds and π-π stacking

interactions. Results comparing the most stable structure for each disposition and complex are displayed in Table 1. As it can be seen, the parallel arrangement is the most favored, the antiparallel one being destabilized by 3.0 and 4.1 kcal/mol for the complexes with three and four FFF strands, respectively. These results are fully consistent with the parallel-alignment experimentally observed in helical channels of FF nanotubes, which were found to be structurally similar to three-dimensional FF crystals.[24] Moreover, the irregular tubular structures of FFFF were also modeled using a parallel-aligned β-strands.[11] In opposition, the parallel disposition predicted by DFT calculations for FFF is in apparent disagreement with the force-field and coarse-grained simulations reported by Tamamis *et al.*[27] and Guo *et al.*[29], respectively. Such empirical methodologies predicted that FFF peptides have a preference to be antiparallel,[27,29] even though the sheets formed during the simulations contained two strands only (*i.e.* sheets with more strands were seldom due to the restricted duration of the simulations and the small number of peptide molecules).

On the other hand, inspection of the interaction energies (Eq 1) displayed in Table 1 indicates that, although the parallel disposition is favored with respect to the antiparallel one, both arrangements are very stable exhibiting $\Delta E_{int} << 0$ kcal/mol. The additive or non-additive character of the intermolecular interactions involved in both dispositions was evaluated by calculating the cooperative energy, ΔE_{coop} (Eqs 2-6). Thus, $\Delta E_{coop} = 0$ kcal/mol when intermolecular interactions are additive, while $\Delta E_{coop} \neq 0$ reflects the existence of cooperative ($\Delta E_{coop} < 0$ kcal/mol) or anti-cooperative ($\Delta E_{coop} > 0$ kcal/mol) effects. The values displayed in Table 1 clearly demonstrate that both the parallel and antiparallel arrangements exhibit cooperative effects, even though these are more stabilizing for the former one. Moreover, these effects become more stabilizing with increasing number of β-strands.

Detailed inspection of the most stable parallel and antiparallel β-sheets (Figures 7 and S8 for model complexes with four and three strands, respectively) reveals important differences in terms of specific interactions. Amazingly, inter-strand hydrogen bonds (*i.e.* N–H···O distance < 2.5 Å) are more abundant for the antiparallel β-sheets (9 / 5 for the models with 4 / 3 strands) than for the parallel one (6 / 4 for the models with 4 /3 strands), even though H···O distances are slightly larger for the former than for the latter. However, the most remarkable difference refers to inter-strand π-π stacking interactions, which are formed in parallel β-sheets only. More specifically, face-to-face interacting phenyl rings form three characteristic aromatic ladders in the latter secondary structure (Figure 7a, right). In contrast, aromatic rings remain non-stacked in the antiparallel β-sheets (Figure 7b). These differences explain the higher energy of the antiparallel arrangement with respect to the parallel one, even though both dispositions are very stable, as demonstrate their ΔE_{int} and ΔE_{coop} values (Table 1). Within this context, it should be mentioned that π-π stacking interactions are poorly reproduced by both classical force-field and coarse-grained potentials. This feature, together with the restricted duration of the simulation, may be a possible explanation for the discrepancy between the calculations presented in this work and the simulations reported by Tamamis *et al.*[27] and Guo *et al.*[29], respectively.

FTIR spectroscopy has revealed that β-sheets are associated with amide I bands, which occur in the wavenumber range from 1600 cm^{-1} to 1700 cm^{-1}, and arise primarily from stretching vibrations of main chain carbonyl groups. Early investigations suggested that FTIR spectroscopy might be able to distinguish between parallel from antiparallel β-sheets.[50-53] In the latter, the amide I region displays two typical components. The major component has an average wavenumber located at ~1630 cm^{-1}, whereas the minor component appears at ~1695 cm^{-1} is approximately five-fold weaker

than the major one. The 1695 / 1630 intensity ratio has been suggested to be proportional to the percentage of antiparallel arrangement of the β-strands in a β-sheet. For the parallel β-sheet, the amide I region displays only the major component around 1630 cm^{-1}.

Figure 8 displays the amide I regions of the FTIR spectra recorded for the structures derived from 3.5 mg/mL FFF solutions in HFIP:water, HFIP:MeOH and HFIP:^{i}PrOH. For the three environments, the spectrum recorded for undefined peptide structures achieved after rapid evaporation (40 min) in an empty line at room temperature is compared with that of the plate-like microstructures formed after 10 days in 4 ºC chamber. In HFIP:water and HFIP:MeOH, the amide I region is characterized by the presence of a major band at a wavenumber comprised between 1629 and 1646 cm^{-1} and a shoulder or a well-defined band at 1687 cm^{-1}. This feature suggests that parallel β-sheets are preferred when solvent evaporation is fast while the antiparallel disposition when the evaporation of the solvent is slow. The red- and blue-shift observed for the major component of the spectrum recorded after slow solvent evaporation in HFIP:water and HFIP:MeOH, respectively, have been attributed to the presence excitonic coupling effects in the frequency positions.[54] In HFIP:^{i}PrOH, the two spectra were practically identical. This can be attributed to the lack of well-defined assemblies, even after 10 days, at peptide concentrations higher than 2 mg/mL and/or the low-polarity of the HFIP:^{i}PrOH mixture, which is the closest to the gas-phase environment used for the calculations. Interestingly, the shoulder at 1687 cm^{-1} is practically disappeared while the intensity of the major component at 1632 cm^{-1} is very low with respect to those observed in the other two environments.

In summary, DFT calculations on model complexes and FTIR spectra indicate that FFF is able to adopt both parallel and antiparallel β-sheets. However, the former seems

to be preferred in structures formed by kinetically-driven self-assembly processes and/or in non-polar environments, whereas the latter is preferred by thermodynamically formed structures. Although both are very stable, the parallel β-sheet is apparently favored with respect to the antiparallel one due to the formation of inter-strand π-π interactions. However, inter-sheet interactions, which in some cases play a crucial role in the stability of the different packing modes,[44] could reverse this situation. Therefore, more investigation applying more sophisticated models is required to address unambiguously the organization of FFF molecules in supramolecular structures.

CONCLUSIONS

We have demonstrated the unique properties of FFF. The distinctive hierarchical self-assembly of this simple tripeptide is precisely controlled through the balance between peptide···peptide and peptide···solvent interactions, which in turn are regulated by the peptide concentration and the polarity of the solvent mixture used to dissolve the peptide, respectively. The morphological variability obtained by controlling such parameters is enormous and include flat plates, laminated helical fibrils, grouped needle-like structures, doughnut-like hollow shapes, micro-bottles (or stacked toroids), individual and grouped chrysanthemum-like structures, and leaves-like dendrimers. The mechanisms proposed for the formation of such supramolecular structures reflect how structural nucleation and hierarchical growing depend on the dominant role of a given kind of interactions. Considering that these morphologies were obtained at 4 ºC and the low volatility of the solvents mixtures at such temperature, they are expected to be thermodynamically stable. Another distinctive characteristic of FFF is its capacity to form both parallel and antiparallel β-sheets, as has been evidenced by DFT calculations and FTIR spectroscopy.

Overall, the capacity of FFF to assemble in very diverse supramolecular structures is greater to that exhibited by its homologues with an even number of Phe residues (*i.e.* FF and FFFF). This unique behavior is of enormous interest from a technological perspective because different applications can be proposed using a single peptide sequence and regulating unmistakable parameters, such as the concentration and the environmental polarity. Collectively, our findings provide additional insights into peptide structure formation, which would be helpful for designing a variety of versatile morphologies with distinctive characteristics.

SUPPORTING INFORMATION

The Supporting Information is available free of charge on the ACS Publications website: Optical microscopy, SEM and AFM micrographs under different conditions, and structures derived from DFT calculations on complexes with three strands.

ACKNOWLEDGEMENTS

Authors thank supports from MINECO and FEDER (MAT2015-69367-R, MAT2015-69547-R and CTQ2013-40855-R) and Gobierno de Aragón - FEDER (research group E40). Support for the research of C.A. was received through the prize "ICREA Academia" for excellence in research funded by the Generalitat de Catalunya.

REFERENCES

1. Reches, M.; Gazit, E. Casting Metal Nanowires within Discrete Self-Assembled Peptide Nanotubes. *Science* **2003**, *300*, 625–627.
2. Yan, X.; Zhu, P.; Li, J. Self-Assembly and Application of Diphenylalanine-Based Nanostructures. *Chem. Soc. Rev.* **2010**, *39*, 1877–1890.

3. Hamley, I. W. Peptide Nanotubes. *Angew. Chem. Int. Ed.* **2014**, *53*, 6866–6881.
4. Lakshmanan, A.; Zhang, S.; Hauser, C. A. E. Short Self-Assembling Peptides as Building Blocks for Modern Nanodevices. *Trends Biotech.* **2012**, *30*, 155–165.
5. Lakshmanan, A.; Cheong, D. W.; Accordo, A.; Fabrizio, E. Di; Riekel, C.; Hauser, C. A. E. Aliphatic Peptides Show Similar Self-Assembly to Amyloid Core Sequences, Challenging the Importance of Aromatic Interactions in Amyloidosis. *Proc. Natl. Acad. Sci.* **2013**, *110*, 519–524.
6. Marchesan, S.; Waddington, L.; Easton, C. D.; Winkler, D. A.; Goodall, L.; Forsythe, J.; Hartley, P. G. Unzipping the Role of Chirality in Nanoscale Self-Assembly of Tripeptide Hydrogels. *Nanoscale* **2012**, *4*, 6752–6760.
7. Fleming, S.; Ulijn, R. V. Design of Nanostructures Based on Aromatic Peptide Amphiphiles. *Chem. Soc. Rev.* **2014**, *43*, 8150–8177.
8. Martin, A. D.; Robinson, A. B.; Thordason, P. Biocompatible Small Peptide Super-Hydrogelators Bearing Carbazole Functionalities. J. *Mater. Chem. B* **2015**, *3*, 2277–2280.
9. Matson, J. B.; Stupp, S. I.; Self-Assembling Scaffolds for Regenerative Medicine. *Chem. Commun.* **2012**, *48*, 26–33.
10. Cavalli, S.; Albericio, F.; Kros, A. Amphiphilic Peptides and Their Cross-Disciplinary Role as Building Blocks for Nanoscience. *Chem. Soc. Rev.* **2010**, *39*, 241-263.
11. Mayans, E.; Ballano, G.; Casanovas, J.; Díaz, A.; Pérez-Madrigal, M. M. ; Estrany, F.; Puiggalí, J.; Cativiela, C.; Alemán, C. Self-Assembly of Tetraphenylalanine Peptides. *Chem. Eur. J.* **2015**, *21*, 16895–16905.
12. Mayans, E.; Ballano, G.; Casanovas, J.; del Valle, L. J.; Pérez-Madrigal, M. M.; Estrany, F.; Jiménez, A. I.; Puiggalí, J.; Cativiela, C.; Alemán, C. Hierarchical Self-

Assembly of Di-, Tri- and Tetraphenylalanine Peptides Capped with Two Fluorenyl Functionalities: From Polymorphs to Dendrites. *Soft Matter* **2016**, *12*, 5475–5488.

13. Reches, M; Gazit, E. Designed Aromatic Homo-Dipeptides: Formation of Ordered Nanostructures and Potential Nanotechnological Applications. *Phys. Biol.* **2006**, *3*, S10–S19.
14. Gazit, E. Self-Assembled Peptide Nanostructures: The Design of Molecular Building Blocks and Their Technological Utilization. *Chem. Soc. Rev.* **2007**, *36*, 1263–1269.
15. Huang, R.; Su, R.; Qi, W.; Zhao, J.; He, Z. Hierarchical, Interface-Induced Self-Assembly of Diphenylalanine: Formation of Peptide Nanofibers and Microvesicles. *Nanotechnology* **2011**, *22*, 245609.
16. Han, T. H.; Ok, T.; Kim, J.; Shin, D. O.; Ihee, H.; Lee, H.-S.; Kim, S. O. Bionanosphere Lithography via Hierarchical Peptide Self-Assembly of Aromatic Triphenylalanine. *Small* **2010**, *6*, 945−951.
17. Azuri, I.; Adler-Abramovich, L.; Gazit, E.; Hod, O.; Kronik, L. Why Are Diphenylalanine-Based Peptide Nanostructures So Rigid? Insights from First Principles Calculations. *J. Am. Chem. Soc.* **2014**, *136*, 963−969.
18. Adler-Abramovich, L.; Kol, N.; Yanai, I.; Barlam, D.; Shneck, R. Z.; Gazit, E.; Rousso, I. Self-Assembled Organic Nanostructures with Metallic-Like Stiffness. *Angew. Chem., Int. Ed.* **2010**, *49*, 9939−9942.
19. Zelenovskiy, P.; Kornev, I.; Vasilev, S.; Kholkin, A. On the Origin of the Great Rigidity of Self-Assembled Diphenylalanine Nanotubes. *Phys. Chem. Chem. Phys.* **2016**, *18*, 29681−29685.

20. Adler-Abramovich, L.; Reches, M.; Sedman, V. L.; Allen, S.; Tendler, S. J. B.; Gazit, E. Thermal and Chemical Stability of Diphenylalanine Peptide Nanotubes: Implications for Nanotechnological Applications. *Langmuir* **2006**, *22*, 1313−1320.
21. Andersen, K. B.; Castillo-Leon, J.; Hedström, M.; Svendsen, W. E. Stability of Diphenylalanine Peptide Nanotubes in Solution. *Nanoscale* **2011**, *3*, 994–998.
22. Semin, S.; van Etteger, A.; Cattaneo, L.; Amdursky, N.; Kulyuk, L.; Lavrov, S.; Sigov, A.; Mishina, E.; Rosenman, G.; Rasing, T. Strong Thermo-Induced Single and Two-Photon Green Luminescence in Self-Organized Peptide Microtubes. *Small* **2015**, *11*, 1156−1160.
23. Gan, Z.; Wu, X.; Zhu, X.; Shen, J. Light-Induced Ferroelectricity in Bioinspired Self-Assembled Diphenylalanine Nanotubes/Microtubes. *Angew. Chem., Int. Ed.* **2013**, *52*, 2055−2059.
24. Görbitz, C. H. Nanotube Formation by Hydrophobic Dipeptides. *Chem. Eur. J.* **2001**, *7*, 5153–5159.
25. Kim, J.; Han, T. H.; Kim, Y.-I.; Park, J. S.; Choi, J.; Churchill, D. G.; Kim, S. O.; Ihee, H. Role of Water in Directing Diphenylalanine Assembly into Nanotubes and Nanowires. *Adv. Mater.* **2010**, *22*, 583–587.
26. Li, Q.; Ma, H.; Jia, Y.; Li, J.; Zhu, B. Facile Fabrication of Diphenylalanine Peptide Hollow Spheres Using Ultrasound-Assisted Emulsion Templates. *Chem. Commun.* **2015**, *51*, 7219–7221.
27. Tamamis, P.; Adler-Abramovich, L.; Reches, M.; Marshall, K.; Sikorski, P.; Serpell, L.; Gazit, E.; Archontis, G. Self-Assembly of Phenylalanine Oligopeptides: Insights from Experiments and Simulations. *Biophys. J.* **2009**, *96*, 5020–5029.
28. Guo, C.; Arnon, Z. A.; Qi, R.; Zhang, Q.; Adler-Abramovich, L.; Gazit, E.; Wei, G. Expanding the Nanoarchitectural Diversity Through Aromatic Di- and Tri-Peptide

Coassembly: Nanostructures and Molecular Mechanisms. *ACS Nano* **2016**, *10*, 8316−8324.

29. Guo, C.; Luo, Y.; Zhou, R.; Wei, G. Triphenylalanine Peptides Self-Assemble into Nanospheres and Nanorods that Are Different from the Nanovesicles and Nanotubes Formed by Diphenylalanine Peptides. *Nanoscale* **2014**, *6*, 2800−2811.
30. Castelletto, V.; Hamley, I. W. Self-Assembly of a Model Amphiphilic Phenylalanine Peptide/Polyethylene Glycol Block Copolymer in Aqueous Solution. *Biophys. Chem.* **2009**, *141*, 169−174.
31. Zanuy, D.; Hamley, I. W.; Alemán, C. Modeling the Tetraphenylalanine-PEG Hybrid Amphiphile: From DFT Calculations on the Peptide to Molecular Dynamics Simulations on the Conjugate. *J. Phys. Chem. B* **2011**, *115*, 8937−8946.
32. Tzokova, N.; Fernyhough, C. M.; Topham, P. D.; Sandon, N.; Adams, D. J.; Butler, M. F.; Armes, S. P.; Ryan, A. J. Soft Hydrogels from Nanotubes of Poly(ethylene oxide)−Tetraphenylalanine Conjugates Prepared by Click Chemistry. *Langmuir* **2009**, *25*, 2479−2485.
33. Gaussian 09, Revision A.02, Frisch, M. J.; Trucks, G. W.; Schlegel, H. B.; Scuseria, G. E.; Robb, M. A.; Cheeseman, J. R.; Scalmani, G.; Barone, V.; Mennucci, B.; Petersson, G. A.; Nakatsuji, H.; Caricato, M.; Li, X.; Hratchian, H. P.; Izmaylov, A. F.; Bloino, J.; Zheng, G.; Sonnenberg, J. L.; Hada, M.; Ehara, M.; Toyota, K.; Fukuda, R.; Hasegawa, J.; Ishida, M.; Nakajima, T.; Honda, Y.; Kitao, O.; Nakai, H.; Vreven, T.; Montgomery, J. A., Jr.; Peralta, J. E.; Ogliaro, F.; Bearpark, M.; Heyd, J. J.; Brothers, E.; Kudin, K. N.; Staroverov, V. N.; Kobayashi, R.; Normand, J.; Raghavachari, K.; Rendell, A.; Burant, J. C.; Iyengar, S. S.; Tomasi, J.; Cossi, M.; Rega, N.; Millam, J. M.; Klene, M.; Knox, J. E.; Cross, J. B.; Bakken, V.; Adamo, C.; Jaramillo, J.; Gomperts, R.; Stratmann, R. E.;

Yazyev, O.; Austin, A. J.; Cammi, R.; Pomelli, C.; Ochterski, J. W.; Martin, R. L.; Morokuma, K.; Zakrzewski, V. G.; Voth, G. A.; Salvador, P.; Dannenberg, J. J.; Dapprich, S.; Daniels, A. D.; Farkas, Ö.; Foresman, J. B.; Ortiz, J. V.; Cioslowski, J.; Fox, D. J. Gaussian, Inc., Wallingford CT, 2009.

34. Zhao, Y.; Truhlar, D. G. The M06 Suite of Density Functionals for Main Group Thermochemistry, Thermochemical Kinetics, Noncovalent Interactions, Excited States, and Transition Elements: Two New Functionals and Systematic Testing of Four M06-Class Functionals and 12 Other Functionals. *Theor. Chem. Acc.* **2008**, *120*, 215−241.
35. Zhao, Y.; Truhlar, D. G. A New Local Density Functional for Main-Group Thermochemistry, Transition Metal Bonding, Thermochemical Kinetics, and Noncovalent Interactions. *J. Chem. Phys.* **2006**, *125*, 194101.
36. Tzokova, N.; Fernyhough, C. M.; Butler, M. F.; Armes, S. P.; Ryan, A. J.; Topham, P. D.; Adams, D. J. The Effect of PEO Length on the Self-Assembly of Poly(ethylene oxide)−Tetrapeptide Conjugates Prepared by "Click" Chemistry. *Langmuir* **2009**, *25*, 11082−11089.
37. Tao, K.; Levin, A.; Adler-Abramovich, L.; Gazit, E. Fmoc-Modified Amino Acids and Short Peptides: Simple Bio-Inspired Building Blocks for the Fabrication of Functional Materials. *Chem. Soc. Rev*. **2016**, *45*, 3935−3953.
38. Fichman, G; Gazit, E. Self-Assembly of Short Peptides to Form Hydrogels: Design of Building Blocks, Physical Properties and Technological Applications. *Acta Biomater*. **2014**, *10*, 1671−1682.
39. Cai, C. H.; Lin, J. P.; Lu, Y. Q.; Zhang, Q.; Wang, L. Q. Polypeptide Self-Assemblies: Nanostructures and Bioapplications, *Chem. Soc. Rev.* **2016**, *45*, 5985−6012.

40. Lu, K.; Jacob, J.; Thiyagarajan, P.; Conticello, V. P.; Lynn, D. G. Exploiting Amyloid Fibril Lamination for Nanotube Self-Assembly. *J. Am. Chem. Soc.* **2003**, *125*, 6391−6393.

41. Gordon, D.; Meredith, S. C. Probing the Role of Backbone Hydrogen Bonding in β-Amyloid Fibrils with Inhibitor Peptides Containing Ester Bonds at Alternate Positions. *Biochemistry* **2003**, *42*, 475−485.

42. Burkoth, T. S.; Benzinger, T. L. S.; Urban, V.; Morgan, D. M.; Gregory, D. M.; Thiyagarajan, P.; Botto, R. B; Meredith, S. C.; Lynn, D. G. Structure of the β-Amyloid$_{(10\text{-}35)}$ Fibril. *J. Am. Chem. Soc.* **2000,** *122*, 7883−7889.

43. Kirschner, D. A.; Inouye, H.; Duffy, L. K.; Sinclair, A.; Lind, M.; Selkoe, D. J. Synthetic Peptide Homologous to β Protein from Alzheimer Disease Forms Amyloid-Like Fibrils *In Vitro*. *Proc. Natl. Acad. Sci. U.S.A.* **1987**, *84*, 6953−6957.

44. Prakongpan, S.; Nagai, T. Solubility of Acetaminophen in Cosolvents. *Chem. Pharm. Bull.* **1984**, *32*, 340–343.

45. Chien, Y.W. Solubilization of Metronidazole by Water Miscible Multi-Cosolvents and Water-Soluble Vitamins. *J. Parent. Sci. Technol.* **1984**, *38*, 32–36.

46. Jouyban, A.; Soltanpour, S.; Chan, H.-K. A Simple Relationship between Dielectri Constant of Mixed Solvents with Solvent Composition and Temperature. *Int. J. Pharm.* **2004**, *269*, 353–36.

47. Alemán, C. On the Ability of Modified Peptide Links to Form Hydrogen Bonds. *J. Phys. Chem. A* **2001,** *105*, 6717–6723.

48. Sinnokrot, M. O.; Valeev, E. F.; Sherrill, C. D. Estimates of the Ab Initio Limit for π-π Interactions: The Benzene Dimer". J. Am. Chem. Soc. **2002**, *124*, 10887–10893.

49. Zanuy, D.; Poater, J.; Solà, M.; Hamley, I. W.; Alemán, C. Fmoc–RGDS Based Fibrils: Atomistic Details of Their Hierarchical Assembly. *Phys. Chem. Chem. Phys.* **2016**, *18*, 1265–1278.

50. Toniolo, C.; Palumbo, M. Solid-State Infrared Absorption Spectra and Chain Arrangement in Some Synthetic Homooligopeptides in the Intermolecularly Hydrogen-Bonded Pleated-Sheet β-conformation. *Biopolymers* **1977**, *16*, 219–224.

51. Krimm, S.; Bandekar, J. Vibrational Spectroscopy and Conformation of Peptides, Polypeptides, and Proteins. *Adv. Protein Chem.* **1986**, *38*, 181–364.

52. Khurana, R.; Fink, A. L. Do Parallel Beta-Helix Proteins Have a Unique Fourier Transform Infrared Spectrum?. *Biophys. J.* **2000**, *78*, 994–1000.

53. Goormaghtigh, E.; Cabiaux, V.; Ruysschaert, J.-M. Determination of Soluble and Membrane Protein Structure by Fourier Transform Infrared Spectroscopy. I. Assignments and Model Compounds. *Subcell. Biochem.* **1994**, *23*, 329–362.

54. Polzi, L. Z.; Amadei, A.; Aschi, M.; Daidone, I. New Insight into the IR-Spectra/Structure Relationship in Amyloid Fibrils: A Theoretical Study on a Prion Peptide. *J. Am. Chem. Soc.* **2011**, *133*, 11414–11417.

CAPTIONS TO FIGURES

Figure 1. Microstructures obtained by self-assembly from FFF solutions in HFIP:water at 4ºC. (a) SEM micrograph and height AFM image (15×15 μm^2) of microplates from 2 mg/mL peptide solutions (4:6 HFIP:water). (b) Low and high magnified SEM micrographs of twisted microplates from 0.5 mg/mL peptide solutions (1:9 HFIP:water). (c) SEM micrographs of helical ribbons from 0.05 mg/mL peptide solutions (1:99 HFIP:water).

Figure 2. Microstructures obtained by self-assembly from FFF solutions in HFIP:MeOH at 4 ºC. (a) OM and SEM micrographs with increasing magnification of supramolecular microstructures formed by organized nanoplates, which have been derived from 4 mg/mL peptide solutions (4:1 HFIP:MeOH). (b) 3D topographic and 2D height AFM images (15×15 μm^2) of needle-like microstructures displayed in (a).

Figure 3. (a) Scheme summarizing the influence of the polarity of the medium in the assembly of FFF molecules and subsequent organization in plate-containing structures. (b) Scheme illustrating the hierarchical formation of chrysanthemum-like clusters from the assembly of FFF microplates obtained in HFIP:^{i}PrOH using moderate and low peptide concentrations.

Figure 4. Microstructures obtained by self-assembly from FFF solutions in HFIP:MeOH at 4ºC. (a) SEM micrographs and AFM image (3×3 μm^2) of doughnut-like microstructures obtained using a 0.05 mg/mL peptide solution (1:99 HFIP:MeOH). High resolution SEM images reflect the considerable variability of the wall-thickness. (b) 3D topographic and 2D height AFM images (left: 20×20 μm^2; middle and right: 10×10 μm^2) of micro-bottles formed using a 0.05 mg/mL peptide solution (1:99 HFIP:MeOH).

Figure 5. Microstructures obtained by self-assembly from 4 mg/mL FFF solutions in 4:1 HFIP:^{i}PrOH at 4ºC: (a) OM micrographs of coexisting leave-like dendritic and doughnut-like hollow microstructures; (b) SEM micrographs and both height and 3D topographic AFM images (20×20 μm^2) of representative hollow microstructures; and (c) Schematic representation of the mechanism proposed for the self-assembly into doughnut-shape microstructures.

Figure 6. Microstructures obtained by self-assembly from FFF solutions in HFIP:^{i}PrOH at 4ºC. SEM micrographs illustrate different stages in the hierarchical formation of flower-shape microstructures obtained using (a) 2 mg/mL (4:6 HFIP:^{i}PrOH) and (b) 0.5 mg/mL (1:9 HFIP:^{i}PrOH) peptide solutions. The former peptide concentration gives place to very well defined chrysanthemum-like clusters, which are formed through the mechanism depicted in Figure 3b, while the morphology becomes less defined for the latter peptide concentration.

Figure 7. Lowest energy complex with four FFF molecules (two views) obtained considering (a) parallel and (b) antiparallel β-sheets. H···O distances (in Å) are displayed for N – H···O hydrogen bonds. Arrows in (a) indicate the three π-π ladders (indicated with different colors) formed by the stacked phenyl rings.

Figure 8. FTIR spectra in the amide I region of structures derived from 3.5 mg/mL FFF solutions in 3:1 (a) HFIP:water, (b) HFIP:MeOH and (c) HFIP:^{i}PrOH. For (a) and (b) the spectra recorded for structures formed under fast (40 min) and slow (10 days) solvent evaporation conditions are displayed. For (c) the spectra recorded for such two conditions were practically identical and, therefore, only that obtained after slow evaporation is displayed.

Table 1. Relative, interaction and cooperative energies (ΔE, ΔE_{int} and ΔE_{coop}, respectively) calculated for complexes with three and four FFF molecules (Figures 7 and S8, respectively).

System	β-sheet	ΔE (kcal/mol) [a]	ΔE_{int} (kcal/mol) [b]	ΔE_{coop} (kcal/mol) [c]
3 × FFF	Parallel	0.0	-43.9	-2.9
	Antiparallel	3.0	-40.9	-2.2
4 × FFF	Parallel	0.0	-68.9	-7.4
	Antiparallel	4.1	-64.8	-6.9

[a] Relative energy: $\Delta E = E_{parallel} - E_{antiparallel}$. [b] Calculated according to Eq. 1. [c] Calculated according to Eq. 2.

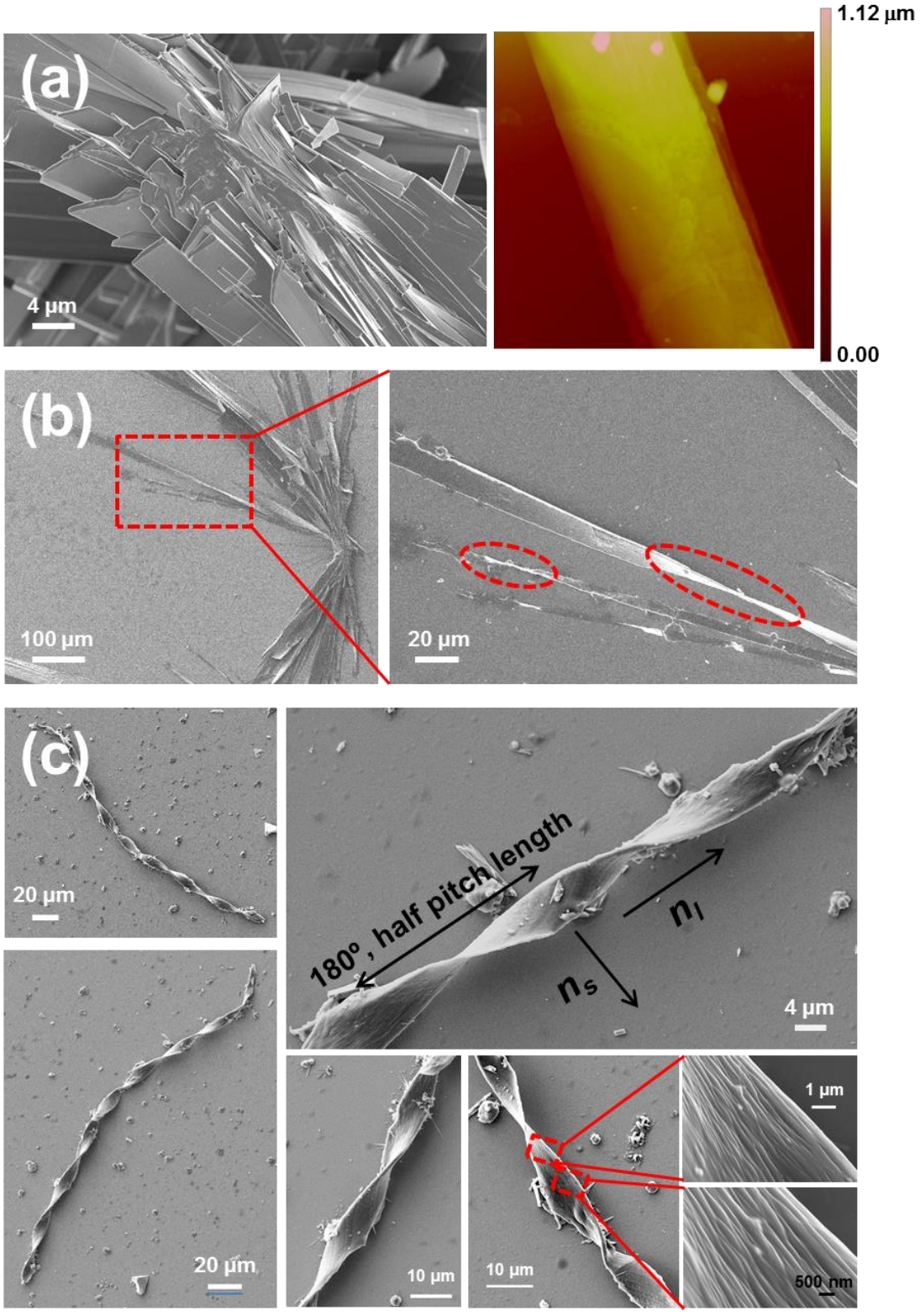
(a)
4 μm
1.12 μm
0.00
(b)
100 μm
20 μm
(c)
20 μm
180°, half pitch length
n_l
n_s
4 μm
20 μm
10 μm
10 μm
1 μm
500 nm

Figure 1

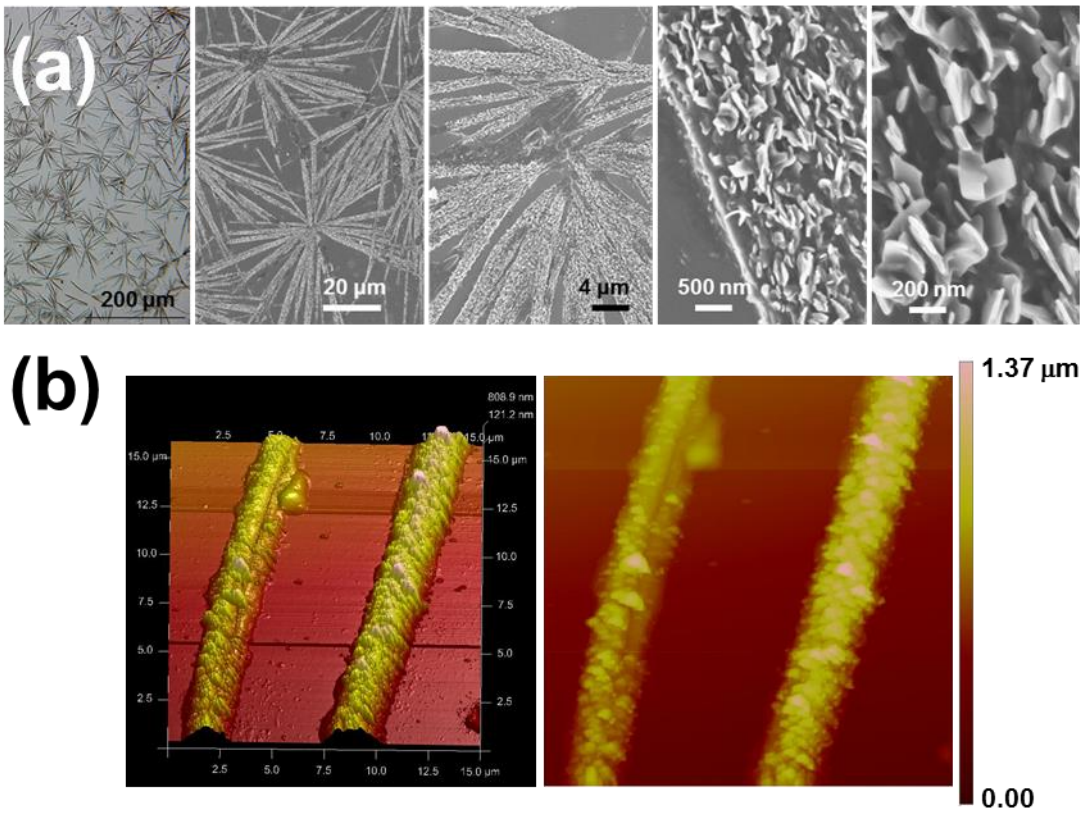

Figure 2

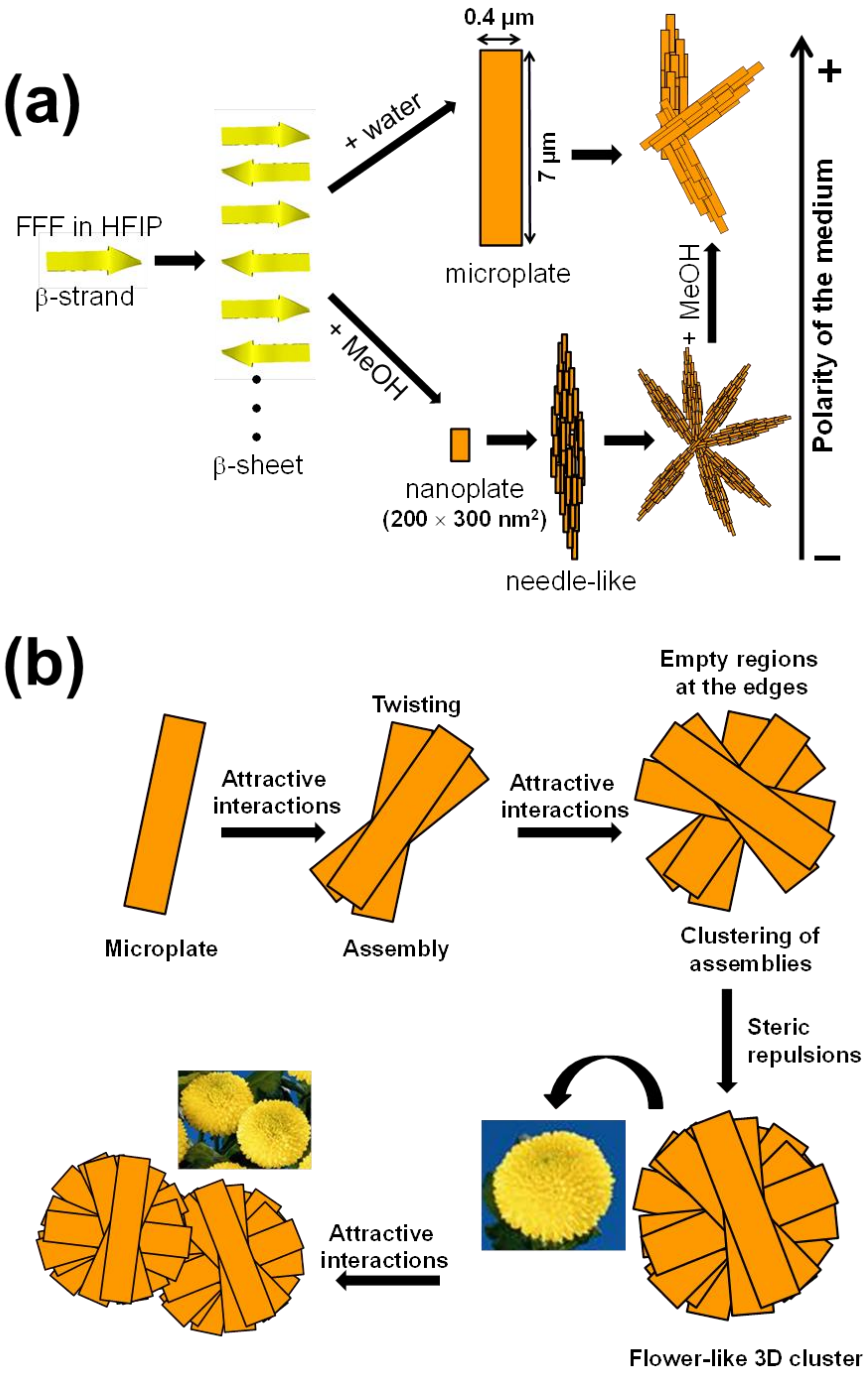
(a)
FFF in HFIP
β-strand
β-sheet
+ water
+ MeOH
0.4 µm
7 µm
microplate
nanoplate
(200 × 300 nm²)
needle-like
+ MeOH
Polarity of the medium
+
–
(b)
Microplate
Attractive interactions
Twisting
Assembly
Attractive interactions
Empty regions at the edges
Clustering of assemblies
Steric repulsions
Flower-like 3D cluster
Attractive interactions

Figure 3

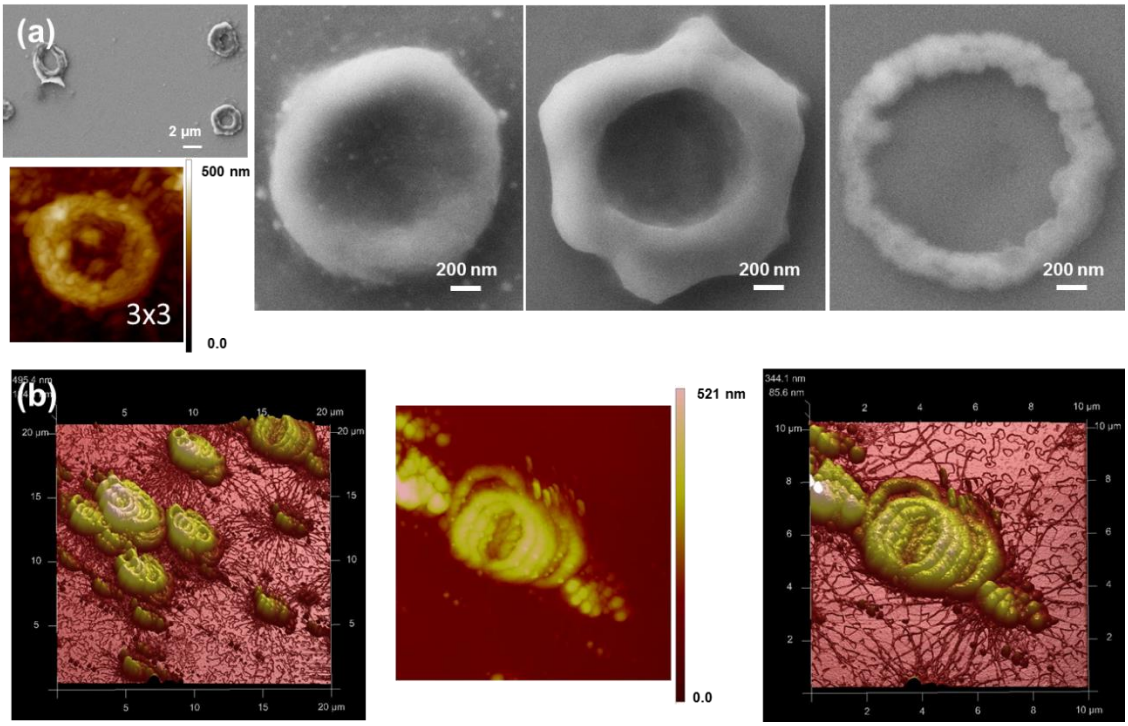

Figure 4

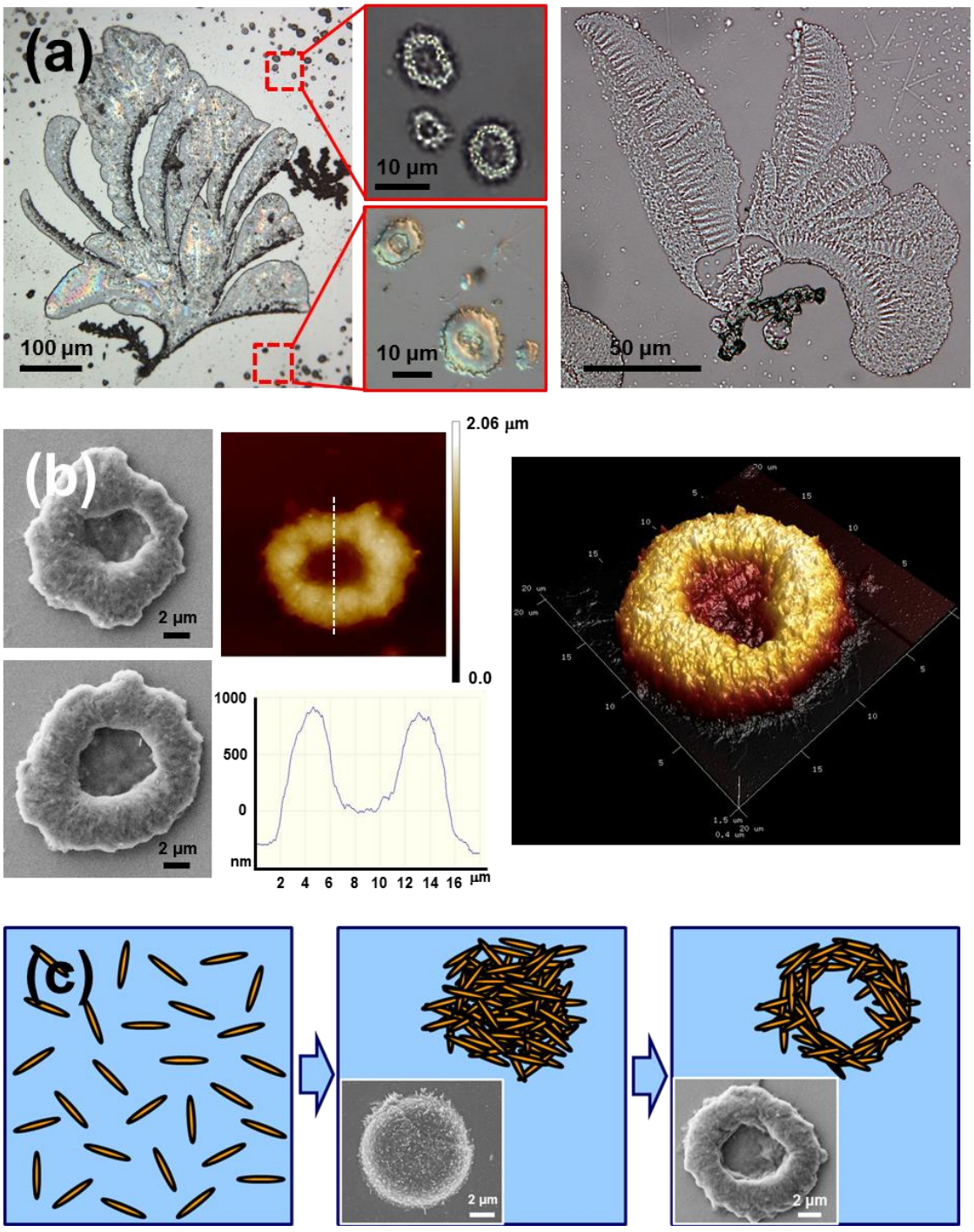
(a)
100 µm
10 µm
10 µm
30 µm
(b)
2 µm
2.06 µm
0.0
2 µm
1000
500
0
nm
2 4 6 8 10 12 14 16 µm
(c)
2 µm
2 µm

Figure 5

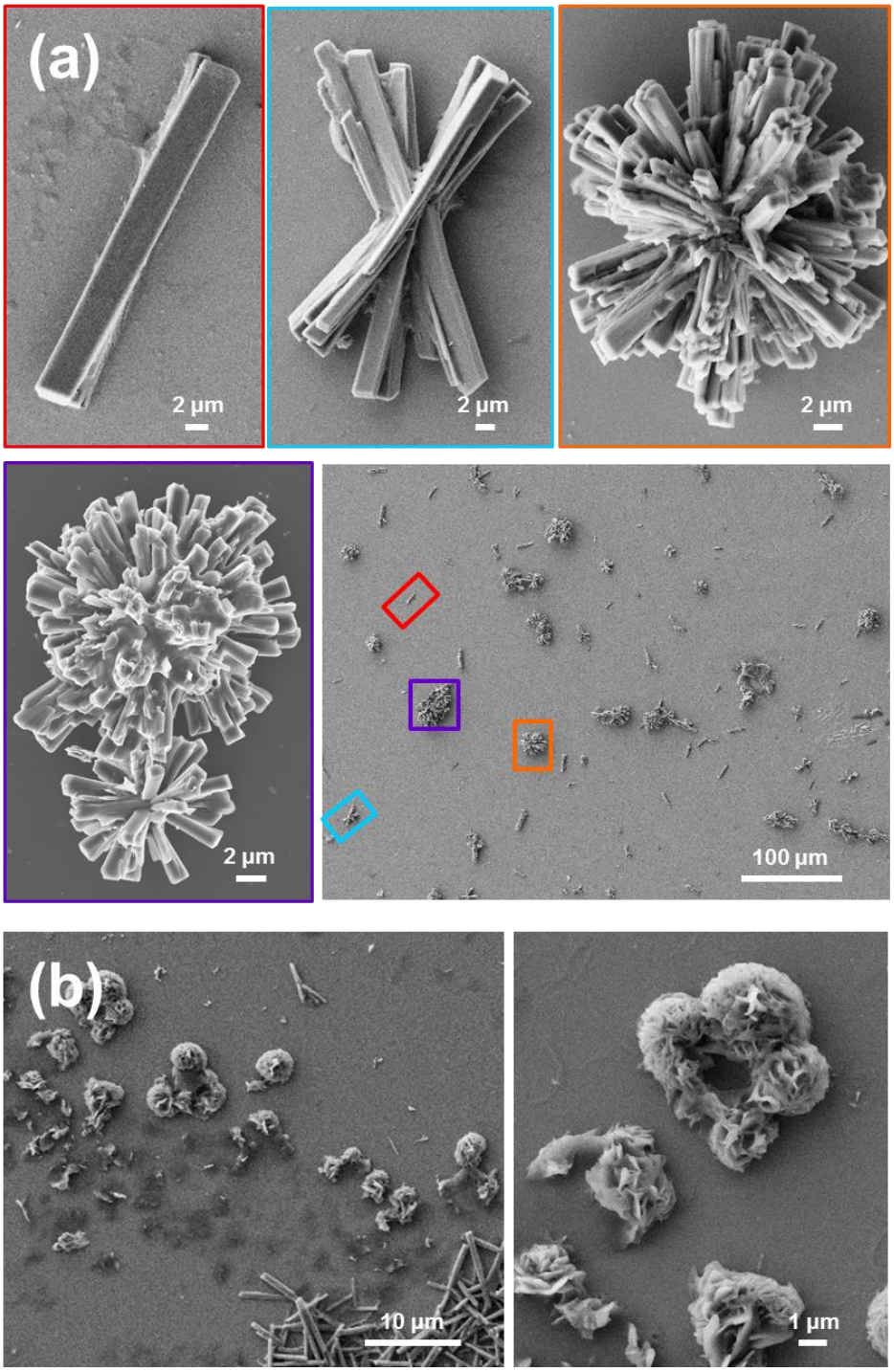

Figure 6

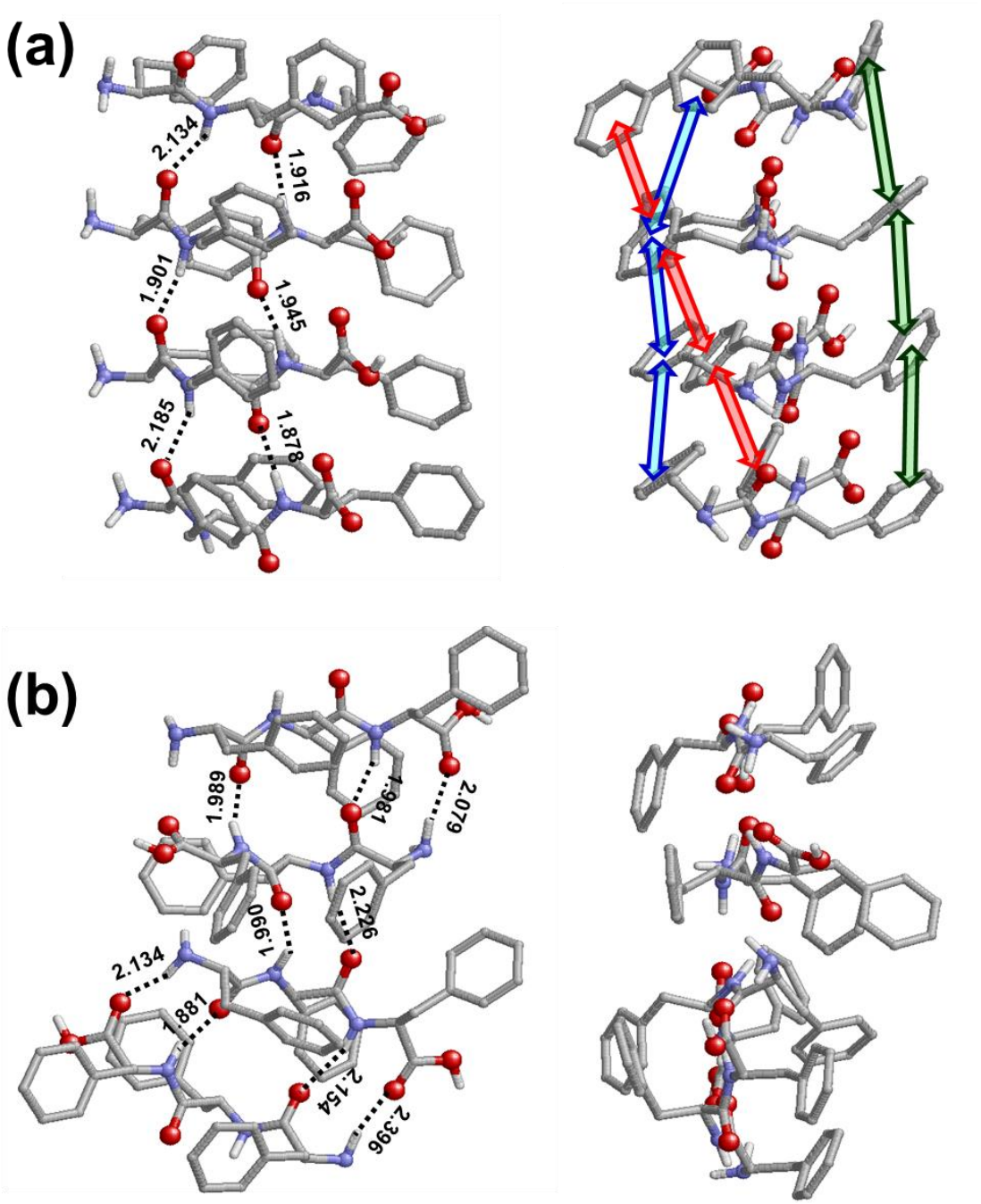
(a)
2.134
1.916
1.901
1.945
2.185
1.878
(b)
1.989
1.981
2.079
1.990
2.226
2.134
1.881
2.154
2.396

Figure 7

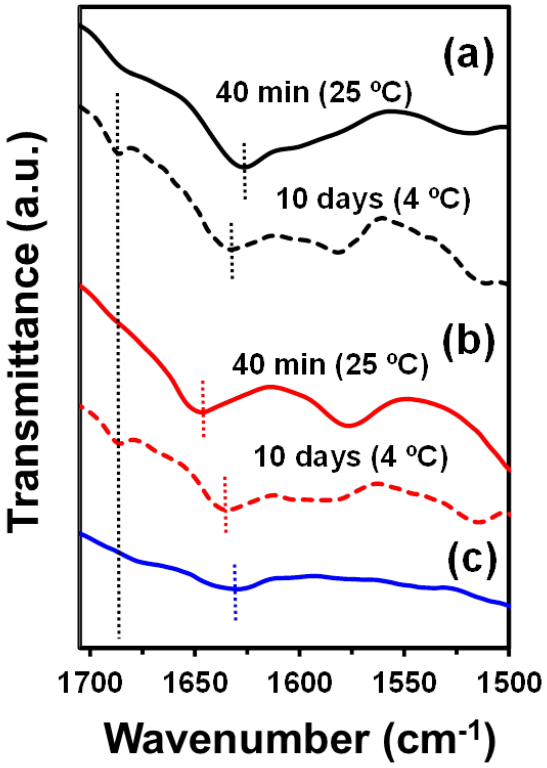
(a)
40 min (25 °C)
10 days (4 °C)
(b)
40 min (25 °C)
10 days (4 °C)
(c)
Transmittance (a.u.)
1700
1650
1600
1550
1500
Wavenumber (cm-1)

Figure 8

TOC